

Article

Exploring Ecological, Morphological, and Environmental Controls on Coastal Foredune Evolution at Annual Scales Using a Process-Based Model

Selwyn S. Heminway ^{1,2,3,*}, Nicholas Cohn ³ , Elizabeth H. Davis ⁴ , Andrew White ^{1,3,5}, Christopher J. Hein ⁴  and Julie C. Zinnert ⁵ 

¹ Oak Ridge Institute for Research and Education, 1299 Bethel Valley Rd, Oak Ridge, TN 37830, USA; aewhite@vcu.edu

² Department of Geology, William & Mary, 200 Stadium Dr., Williamsburg, VA 23185, USA

³ Coastal and Hydraulics Laboratory, U.S. Army Engineer Research and Development Center, 1261 Duck Rd, Kitty Hawk, NC 27949, USA; nicholas.t.cohn@usace.army.mil

⁴ Virginia Institute of Marine Science, William & Mary, 1375 Greate Rd, Gloucester Point, VA 23062, USA; ehdavis@vims.edu (E.H.D.); hein@vims.edu (C.J.H.)

⁵ Department of Biology, Virginia Commonwealth University, 1000 W Cary Street, Richmond, VA 23284, USA; jcziinnert@vcu.edu

* Correspondence: ssheminway@gmail.com



Citation: Heminway, S.S.; Cohn, N.; Davis, E.H.; White, A.; Hein, C.J.; Zinnert, J.C. Exploring Ecological, Morphological, and Environmental Controls on Coastal Foredune Evolution at Annual Scales Using a Process-Based Model. *Sustainability* **2024**, *16*, 3460. <https://doi.org/10.3390/su16083460>

Academic Editors: Yefei Bai,
Peter Sheng, Trevor Meckley,
Karen Thorne and
Vladimir Paramygin

Received: 31 January 2024

Revised: 15 April 2024

Accepted: 19 April 2024

Published: 21 April 2024



Copyright: © 2024 by the authors. Licensee MDPI, Basel, Switzerland. This article is an open access article distributed under the terms and conditions of the Creative Commons Attribution (CC BY) license (<https://creativecommons.org/licenses/by/4.0/>).

Abstract: Coastal communities commonly rely upon foredunes as the first line of defense against sea-level rise and storms, thus requiring management guidance to optimize their protective services. Here, we use the AeoliS model to simulate wind-driven accretion and wave-driven erosion patterns on foredunes with different morphologies and ecological properties under modern-day conditions. Additional sets of model runs mimic potential future climate changes to inform how both morphological and ecological properties may have differing contributions to net dune changes under evolving environmental forcing. This exploratory study, applied to represent the morphological, environmental, and ecological conditions of the northern Outer Banks, North Carolina, USA, finds that dunes experiencing minimal wave collision have similar net volumetric growth rates regardless of beach morphology, though the location and density of vegetation influence sediment deposition patterns across the dune profile. The model indicates that high-density, uniform planting strategies trap sediment close to the dune toe, whereas low-density plantings may allow for accretion across a broader extent of the dune face. The initial beach and dune shape generally plays a larger role in annual-scale dune evolution than vegetation cover. For steeper beach slopes and/or low dune toe elevations, the model generally predicts wave-driven dune erosion at the annual scale.

Keywords: coastal dunes; aeolian transport; coastal erosion; AeoliS; nature-based solutions

1. Introduction

Sea-level rise (SLR) and storms pose substantial risks to low-lying coastal communities through flooding and beach erosion. Climate change will likely exacerbate these coastal hazards, impacting millions of people living in vulnerable, low-lying coastal areas [1]. There is poor consensus on the magnitude of potential SLR over the coming century, with estimates for increases in the global water level for 2100 ranging between 0.3 and 2.0 m [2]. Simultaneously, warming sea-surface temperatures and other environmental factors are likely to contribute to stronger, more intense tropical cyclones and hurricanes in locations such as the southeastern United States [1], which will bring increased coastal flooding and storm surge. Though the frequency of tropical cyclones and hurricane events is expected to decrease in this region [3], the impact of high-magnitude storm events is likely to be magnified by higher background water levels resulting from SLR. Consequently, an altered storm climate will likely increase the number of events that damage valuable infrastructure

in coastal regions. Coastal communities often maintain natural and nature-based features, such as foredunes, to protect landward infrastructure from these coastal hazards [4]. Dunes are also valued for providing ecological and socioeconomic services, including habitat for endangered species, sites of high tourism value, groundwater recharge zones, and coastal safety maintenance [5]. However, both natural and constructed dunes have been shown to be highly vulnerable to erosion, breaching, and over-washing [6], thereby reducing the critical services they provide. Numerous physical and ecological processes, as described below, contribute to the growth or erosion of dune systems at timescales of hours to centuries, affecting their present-day and future protective services.

1.1. Wind-Driven Dune Growth

Dune growth is primarily a result of aeolian (wind-driven) sediment transport from the beach. Wind speeds exceeding the threshold velocity for the initiation of motion are required to commence saltation and, when there is an onshore-directed component of the wind vector, subsequent sand transport into the dune can initiate volumetric dune growth [7]. There are numerous sediment supply limiters related to surface moisture and sediment texture variability that can impact expected transport rates for given wind conditions and influence the length scale—often referred to as the critical fetch length—to achieve saturation of sediment concentrations within the saltation layer (e.g., [8]). Considering that typical field-observed critical fetch lengths required to reach saturation are on the order of tens of meters (e.g., [9]), wider beach states are more likely to achieve transport saturation than narrower beaches. As a result, the tidal phase and beach slope influence the beach width and modulate instantaneous (e.g., hourly) sediment fluxes to the dune. Previous studies showed that beach width is positively correlated with foredune height and width [10,11]. The location of the dune toe, which is a morphological or ecological metric meant to define the boundary where a beach ends and the dune begins, is the typical reference point for which to calculate sediment fluxes entering the dune and contributing to volumetric dune growth. The dune toe elevation can vary widely over local to regional scales (e.g., [12]), with important implications for dune growth and erosion processes. Although total wind-driven sediment fluxes delivered to the dunes is a primary metric of interest to understand the resilience of a system, the sediment aggraded across the dune profile influences the dune shape, and thus has direct implications for future erosion- and flood-protection functions (e.g., [11]).

1.2. Wave-Driven Erosion

Storm impacts on coastal dunes are highly variable alongshore, reflecting local differences in beach and dune properties [13]. Storm impacts range from erosion at the dune toe to foredune inundation and are often quantified (e.g., [14]) based on the local beach and dune morphology in the context of the expected storm-driven still-water level (SWL) and total-water level (TWL). The TWL is a statistical quantity representing a measure of the vertical extent of high-water levels that includes wave setup and swash contributions. Offshore wave conditions, such as wave height and wave period, influence these swash zone processes, including the maximum height of the TWL relative to the toe of the dune (e.g., [15]) and the total volume of storm-driven dune erosion [14,16]. Because higher TWLs generally enhance event-scale dune erosion, higher background SWLs associated with SLR and storm surge will thus amplify volumetric dune erosion through increased frequency of wave collision [17]. However, storms are not necessarily fully erosive agents. For example, changes in storminess could also alter the speed and direction of winds responsible for dune growth [3], thereby increasing sediment fluxes to the dunes, and partially counteracting wave-driven erosion.

1.3. Vegetation Dynamics of Dunes

Shore-perpendicular vegetation density varies across the dune profile and is influenced by the combination of past disturbances and environmental conditions (e.g., [18]).

These environmental forces result in uneven distributions of plants and spatially varying vegetation density and species richness across the dune profile [19].

Vegetation plays a particularly important role in modifying wind-driven sediment transport gradients in natural and managed coastal settings, thus influencing the dune shape [20] and dune response to coastal hazards [21]. Research linking dune morphology to local ecological properties has also demonstrated relationships between the dominant grass species and the style of dune growth [22], e.g., promoting vertical growth versus dune widening. Both the plant species [23] and density characteristics (e.g., [24]) influence trapping rates and patterns. For example, using data from wind tunnel studies and numerical modeling, Dickey et al. [25] showed that vegetation density affected the pattern and magnitude of sediment deposition, where dense vegetation trapped more sediment and closer to the first presence of plants within a patch, relative to low-density plant patches. Many dune vegetation species also respond positively to sand burial [24,26], thus perpetuating a positive feedback cycle of vegetation growth and expansion, and resulting in enhanced dune growth. Dune vegetation not only encourages aeolian deposition but may also reduce erosion during wave collision events [27]. Above-ground vegetation has been shown to slow wave run-up and reduce wave overtopping and over-washing of the foredune [28], while below-ground biomass contributes to sand cohesion and internal dune stability [27]. Both wind- and wave-driven processes, in conjunction with vegetation effects on modifying sand transport patterns, are ultimately important for the net development of dune systems at annual and longer temporal scales (e.g., [29]). Dune growth rates can differ considerably over short spatial scales due to combined effects on management interventions and local morphodynamic controls on aeolian inputs and exports from the dune [30].

Nature-based approaches (such as beach nourishment, sand fencing, wrack line management, and dune vegetation planting) can enhance aeolian deposition and increase dune stability. Vegetation planting guidelines vary based on plant species (e.g., recommended plant spacing ranges from 0.46 to 1.44 m [31]). To achieve the maximum dune width, staggered spacing of species that grow in the prograding zone of the dune is often recommended (e.g., *Ammophila breviligulata*), such that denser vegetation is planted landward, with decreasing vegetation density seaward [31], though this is not always the standard practice. For example, Cape May, New Jersey, applies staggered planting approaches [31], whereas many communities, such as Duck, North Carolina (NC), do not [32]. Patterns of planted dune grasses may differ substantially from those found in nature, and these initial planting conditions have important implications for ecological–sediment interactions [24].

1.4. Previous Modeling Work Synthesizing Physical and Ecological Effects

Optimizing dune management to maximize dune resilience to erosion requires numerical capabilities that synthesize a broad range of scales and processes. This includes the ability to account for both storm-driven dune erosion, which occurs on the timescale of hours, as well as dune recovery and growth, which is usually a slower process acting over years to decades, and resulting from comparatively slower, lower magnitude wind-driven transport [33]. Standalone dune growth models capable of simulating aeolian transport and eco-morphodynamic processes include the Coastal Dune Model [34], Duna [29], AeoliS [35], and DUBEVEG [36]. AeoliS models sediment transport and morphological changes associated with wind-driven sediment transport in coastal systems, including capabilities to introduce supply limitations associated with moisture and sediment texture effects, as well as spatial variability in bed shear stress driven by topographic effects on flow acceleration and by vegetation presence. Recent applications of the AeoliS model have demonstrated capabilities to specifically simulate multi-fraction wind-driven sediment transport [37], barchan and parabolic dunes [38], vegetative effects on sediment trapping [25], and artificial dune evolution [39]. AeoliS aims to characterize the dominant processes contributing to wind-driven dune growth in coastal systems, but it has not directly included marine effects on beach and dune erosion. Conversely, a separate

class of models aims to resolve the morphologic evolution of wave-driven beach and dune evolution using either analytical [14,16] or process-based approaches (e.g., XBeach [29]). Only a few studies have simultaneously resolved marine and aeolian processes in a single framework, including XBeach–Duna [29] and XBeach–CDM–AeoLiS. While these various coupled frameworks demonstrate promise for advancing the quantitative skill of nearshore beach–dune evolution, they are generally computationally demanding, are subject to compounding feedback errors over extended timeframes (>seasonal), and/or do not account for ecological processes. Continued investment into these technologies can greatly advance knowledge on, and optimize the implementation and design of, both traditional and nature-based infrastructure in coastal environments. The need for reliable quantitative tools to simulate coastal dune evolution and associated hazards is particularly necessary in the context of SLR and climate change, which together threaten to alter dune stability and reinforce the desire for ‘hold the line’ strategies as the preferred adaptation strategy for many coastal communities.

1.5. Study Aims

Coastal foredune evolution represents the aggregation of numerous processes operating at a broad range of scales. Advancing quantitative capabilities and understanding of the influence of processes for net landform change is critical for guiding adaptive management, especially in the context of non-stationary environmental forcings under a changing climate. For example, Sweet et al. [2] forecasts a wide range of potential SLR scenarios out to 2100, and a ~5% change in storm intensity by the end of the 21st century is predicted by Knutson et al. [3] within the Atlantic Basin. These environmental changes add additional uncertainty in how dunes may perform in the future, further motivating the need for quantitative frameworks that synthesize the combination of marine, aeolian, and ecological effects on net landform dune evolution.

Our study aims to use a process-based dune evolution model to explore the ecological and morphological properties of beach–dune systems that enhance dune resilience to storm impacts and SLR. Specifically, we focus on applying improvements to the AeoliS model, now including both dune growth and erosion capabilities, to conditions found along the coast of the Outer Banks, North Carolina, USA. The goals of this study are to (1) explore the relative roles of environmental forcings, antecedent beach and dune morphology, and ecological properties on annual-scale dune evolution, (2) assess the conditions under which dunes are expected to grow and erode, and (3) examine the nature by which future climate changes may alter present-day behavior. Details of the data inputs and AeoliS model methodology are described in Section 2. Results of the hundreds of modeled simulations are presented in Section 3. Discussions and conclusions are provided in Sections 4 and 5, respectively.

2. Materials and Methods

2.1. Study Site and Field Datasets

The Outer Banks is a wave-dominated chain of long, linear, and narrow-barrier islands located off the NC mainland (Figure 1). The region is microtidal (tidal range ~1 m [40]) and experiences an average significant wave height of about 1 m. High-energy storm events frequent the region, including tropical storms in the late summer and fall (August through September), and extratropical nor’easters during the winter (December through March) [41]. The islands of the Outer Banks are net erosional over multi-decadal timescales [42], which serves as an ongoing threat to landward-situated coastal infrastructure.

Here, we focus on the northern part of the Outer Banks, specifically the stretch from Nags Head to Corolla, an area in which dunes play an important role in modulating ocean-side flooding hazards (Figure 1). The average foreshore beach slope within this region is ~0.13 m/m [40], though it ranges from about 0.05 to 0.2 m/m depending on the local grain size and seasonal wave conditions. Dune toe elevations are generally ~3–4 m relative to the NAVD88 datum (mean high water (MHW) is 0.36 m NAVD88 and mean sea level is

−0.13 m NAVD88), though range from about 2.5 to 4.0 m, with dune heights ranging from 6 to 8 m (e.g., [43]).

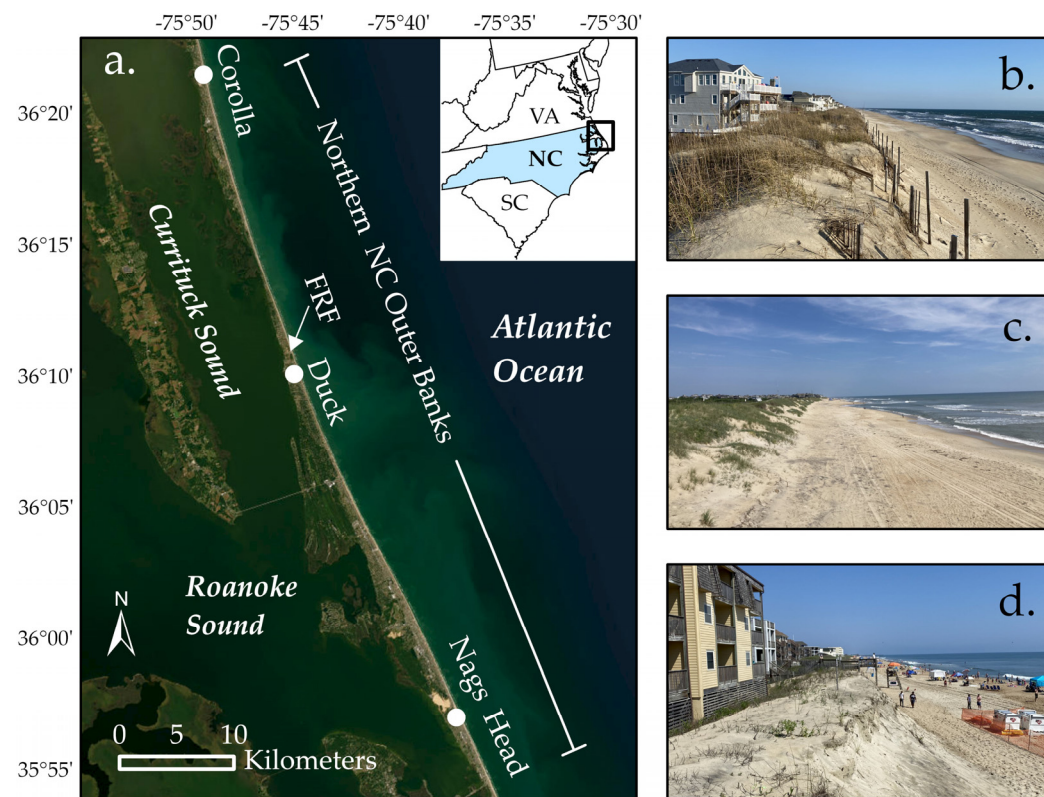


Figure 1. (a) Regional map of the study area along the northern Outer Banks, North Carolina, including the towns of Corolla, Nags Head, and Duck, NC, home of the US Army Corps of Engineers Field Research Facility (FRF). Images represent dunes located in (b) Corolla, (c) Duck, and (d) Nags Head.

Dune vegetation within this coastal reach is unevenly distributed alongshore and across the shore-perpendicular dune profile [43]. Alongshore variation in vegetation density is influenced in part by management interventions carried out by homeowners and town or county managers. At the dune toe, vegetation is typically sparse, whereas the dune crest is densely vegetated [19]. The dune face is an intermediate area of the dune profile, with vegetation densities that vary widely depending on management interventions and past disturbances [18]. Coastal foredunes of the northern Outer Banks are dominated by grasses, lianas, shrubs, and forbs, though our modeling framework focuses on dune grasses. The dominant grass species are distributed across the dune profile in both monocultural and mixed patches, and include *Uniola paniculata*, *Panicum amarum*, *Ammophila breviligulata*, and *Spartina patens*, all of which demonstrate efficient sediment capture and positive growth responses to burial [44].

Ecological data from White [19] consisted of quadrat surveys across our study area in the Outer Banks to determine vegetation density. Shore-perpendicular transects ($n = 4\text{--}16$ transects per site, depending on accessibility) were established at seven sites in the northern Outer Banks in summer 2021. Each transect captured the dune profile from the dune toe to the dune back. Survey plots (0.25 m^2 quadrat) were set along transects in 5 m increments, and vegetation cover was visually estimated as the percentage of vegetation obscuring the bare ground. Statistical analysis was performed to find the range, median, and standard deviation of the vegetation density on the dune face and crest across all sites in our study area.

While dunes in the region have generally experienced recent short-term (sub-decadal) growth (e.g., [43,45]), over decadal and longer time periods the dunes have generally

retreated in response to the cumulative effects of multiple major storms, a retreating shoreline, and SLR [46,47]. Moreover, these dunes are at risk from the impacts of projected climate changes: although future storm patterns remain difficult to predict, the northern Outer Banks lie within the National Oceanic and Atmospheric Administration (NOAA) Southeast Regional SLR Zone, where one of the following SLR scenarios is predicted by 2100: 0.3 m (low) to 0.5 m (intermediate-low), 1.0 m (intermediate), 1.5 m (intermediate-high), or 2.0 m (high) [2].

2.2. Numerical Model Description

AeoLiS [35] is a process-based numerical model that simulates spatiotemporally variable aeolian sediment transport in supply-limited systems. The model uses a Bagnold-type formulation to predict instantaneous sediment concentrations that are dependent on local bed moisture and grain-size characteristics through a modified threshold velocity input. Similar to the Coastal Dune Model of Durán and Moore [34], the implementation of vegetation–wind interaction is modeled according to the expression by Raupach et al. [48]:

$$\frac{u_{*, veg}}{u_*} = \frac{1}{\sqrt{1 + \Gamma \rho_{veg}}} \quad (1)$$

where the ratio of the shear velocity in the presence of vegetation ($u_{*, veg}$) to the unimpeded shear velocity (u_*) is a function of a vegetation-related roughness parameter (Γ) and the vegetation cover within a unit area (ρ_{veg}). The implementation of Raupach et al.'s expression [48] is calculated on each model grid cell based on the local ρ_{veg} , where higher vegetation cover results in a larger decrease in shear velocity relative to sparse vegetation. Collectively, the implementation of these physical and ecological processes into AeoliS enables the simulation of spatial patterns in time-variable sediment transport and morphological changes from wind-driven processes in coastal environments.

In addition to the capability of solving for subaerial eco-morphodynamics that contribute to the growth of coastal foredunes, an analytical dune-erosion model based on wave impact theory was also recently incorporated into the AeoliS framework to account for volumetric dune volume losses and associated erosional dune profile changes due to wave impacts. To characterize if waves contact the dune face, an empirical estimate of wave run-up is first calculated. Wave run-up ($R_{2\%}$), i.e., the elevation exceeded by only 2% of swash excursions, is first calculated based on model inputs of significant wave height (H_s), peak wave period (T_p), and beach slope ($\tan\beta$), following the approach of Stockdon et al. [15]:

$$R_{2\%} = 1.1(0.35\tan\beta \left(H_s \frac{g T_p^2}{2\pi} \right)^{\frac{1}{2}} + \frac{[H_s \frac{g T_p^2}{2\pi} (0.563(\tan\beta)^2 + 0.004)]^{\frac{1}{2}}}{2}) \quad (2)$$

The maximum instantaneous water levels are a function of offshore sea-level fluctuations driven by tides, storm surge, and other non-tidal residual effects, usually summed together as the SWL, and these wave run-up effects operate at the shoreline. Total water levels are then calculated:

$$TWL = SWL + R_{2\%} \quad (3)$$

Ultimately, the amount of sediment removed from the dune during collision is dependent on the force of water making contact with the dune face. The parametric erosion module calculates volumetric erosion using the formula presented by Palmsten and Holman [14]:

$$V = 4C_s(TWL - z_{toe})^2 N_c \quad (4)$$

where C_s is a dune erodibility coefficient, z_{toe} is the dune toe elevation, and N_c is the number of bore collisions making impact with the dune face over a particular time period. Volume losses from the dune are calculated at each model time step (1 h in this application) and removed from the profile at the cell(s) landward of the dune toe contour

elevation. Avalanching based on an angle of repose criteria is imposed, which here limits the development of vertical scarps due to these collisional losses.

Validation of this dune-erosion approach has been completed in the northern Outer Banks [47]. The addition of this capability allows for the inclusion of both relevant marine and aeolian dynamics of dune erosion and dune growth within a single model framework. These combined capabilities were used to forecast the future morphological evolution of foredunes at our study site. Further details of AeoliS can be found at: <https://aeolis.readthedocs.io> (accessed 1 June 2022) and model version 2.1.1 [49] was used in this study.

2.3. Modeling Management Strategies

2.3.1. Baseline Scenario

The model was applied to representative conditions for the coastline of the northern Outer Banks to isolate environmental, morphological, and ecological controls on dune volume changes due to both marine and aeolian processes. For simplicity, we chose a one-year time period over which to simulate and assess magnitudes and patterns in volumetric dune changes, as this is a timescale over which both storm-driven erosion and aeolian transport into the dune complex are relevant. Within the Town of Duck, $\tan\beta$ has been shown to average about 0.1 m/m and typical z_{toe} was 3.0 m NAVD88. However, considering the wide range of measured beach properties in the region of interest (e.g., [50]), subsequent simulations were run for seven values of $\tan\beta$ ranging from 0.05 to 0.2 m/m. Similarly, available morphological datasets (e.g., [45]) from the Outer Banks also demonstrate wide variability in z_{toe} ; thus, nine values of z_{toe} , ranging from 2 to 4 m NAVD88, were assessed in this work. Together, this provided a matrix of 63 total combinations of $\tan\beta$ and z_{toe} . Because these beach state and dune toe conditions have important implications for wind-driven dune growth and wave-driven dune erosion [15,33], use of these wide ranges of pre-existing morphologies allows us to further generalize our findings beyond the short-term conditions observed along the northern Outer Banks. Synthetic beach-dune profiles with a grid size (dx) resolution of 0.5 m were generated with these properties, assuming linear beach and dune slopes and a flat dune crest elevation at 6 m NAVD88. For simplicity, the initial dune top was assumed as a constant elevation that extended 20 m landward from the dune crest. To leverage gradient lateral boundary conditions to account for alongshore wind effects, 2D AeoliS simulations, including three alongshore cells with alongshore uniform topography, were generated from each of these synthetic profiles.

Each of the models was forced with waves, tides, wind speed, and wind direction. Locally measured SWL were sourced from a NOAA tide gauge located at the end of a pier that extends into the Atlantic Ocean at the US Army Engineer Research Development Center (ERDC) Field Research Facility (FRF) in Duck. A continuous hourly time series of SWLs was generated for the period from 1 January to 31 December 2019, which included Hurricane Dorian, a recent storm of record to impact this coast. To develop a generic framework representative for the region, an offshore wave time series for the same annual timeframe for input to AeoliS was sourced from the Wave Information Studies (WIS) hindcast (Node 63218). The H_s , T_p , and calculated TWLs were used by the model to (1) account for time-varying exposed (dry) beach for aeolian transport calculations and (2) for inclusion in the AeoliS dune-erosion module [15]. A continuous 10 m elevation wind time series was sourced from WIS. Wind directions were transformed into a shore-normal coordinate system assuming a shoreline angle of 67.7° relative to north. Offshore-directed winds and any associated seaward sediment fluxes were not considered and were removed in the time series by setting the wind speed for these time periods to below the threshold velocity. The resulting environmental conditions, henceforth referred to as modern-day conditions (Figure 2, black), were run for each of the 63 morphological cases. This matrix of runs was repeated for a number of ecological configurations based on field observations (Section 2.1) to better understand the importance of vegetation densities and distributions on sediment trapping and dune resilience to erosion at the annual timescale. For the “baseline” set of conditions, we assumed a uniform ρ_{veg} of 30% at all grid cells above z_{toe} .

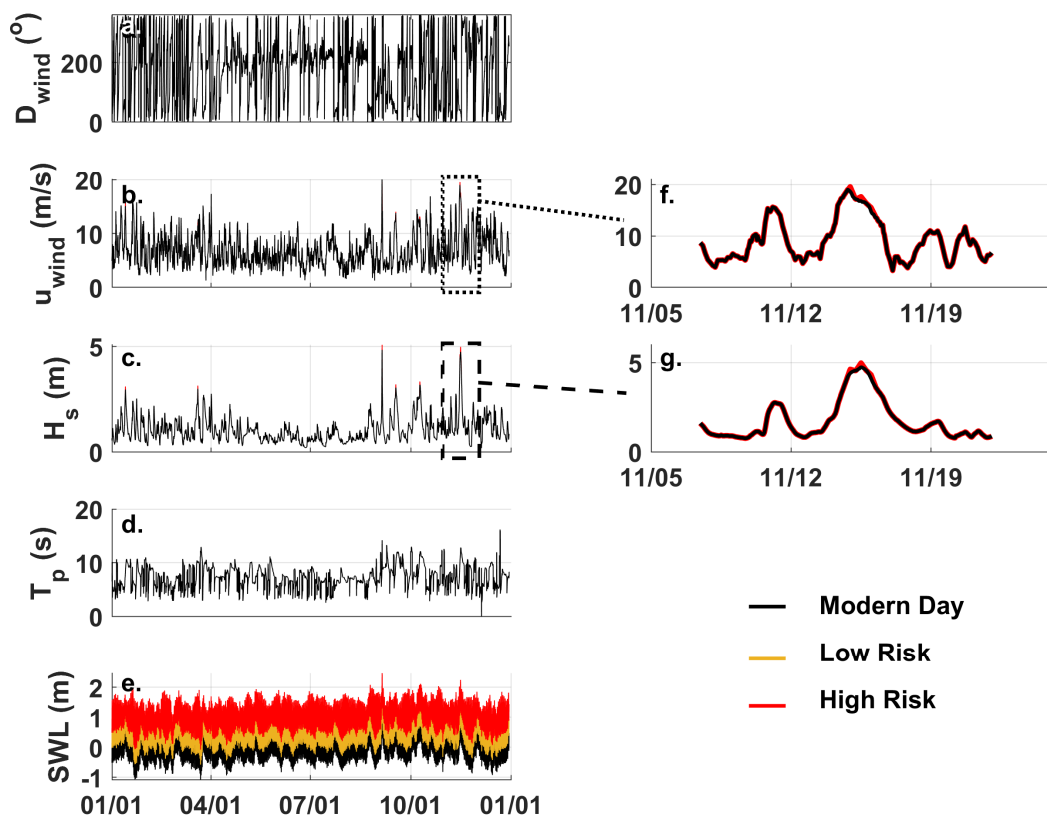


Figure 2. Model inputs (i.e., (a) wind direction, (b) wind speed, (c) significant wave height, (d) peak wave period, and (e) still-water level) modified to create modern-day (black), low-risk (yellow), and high-risk (red) climate states, including an example of an intensified storm (g,f).

To focus on exploration in trends, model defaults for AeoliS were primarily assumed (with limited exceptions), and local model tuning was not conducted. We applied the default aeolian transport coefficient (C_b) of 1.5 for the Bagnold equation for instantaneous sediment concentrations, an hourly model time step, and the Raupach et al. [48] vegetation shear coupler. A spatially and temporally constant grain size of 0.3 mm was applied, corresponding to typical sediment textures for dunes in this region (e.g., [51]). The C_s dune erodibility coefficient, found for a previous application of the Palmsten and Holman [14] dune-erosion model to the Outer Banks by Cohn et al. [47], was used for the erosion module in AeoliS. For this application, the shear module accounting for flow acceleration over dune topography was not utilized due to exceedance of the low-slope assumptions for these dune morphologies. The bed elevation was output at hourly intervals across the whole grid. The net dune volume change was calculated from bed elevation changes above the dune toe to the landward extent of the grid across the entire one-year simulation period.

In the following subsections, we describe additional simulations, in which ecological properties (Section 2.3.2) and environmental conditions (Section 2.3.3) were modified to account for future potential climate conditions, and these are schematized in Figure 3. In total, 1323 AeoliS simulations were run to replicate these various morphological, ecological, and environmental properties.

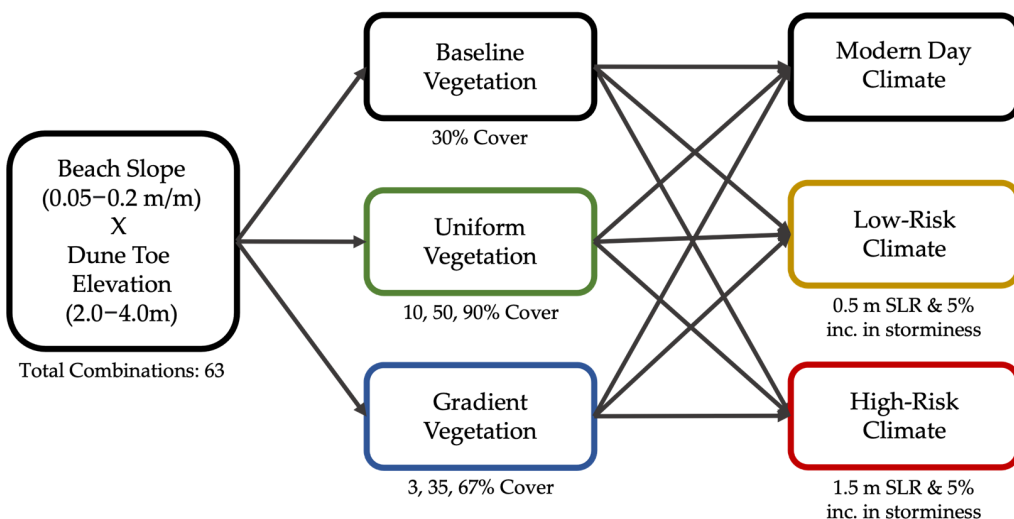


Figure 3. Flow chart of different dune morphologies, vegetation densities, and climate states modeled using AeoliS.

2.3.2. Modeling Dune Grass Planting Strategies

All baseline model runs used a constant 30% ρ_{veg} on the dune face, as previously described. However, natural dune vegetation densities vary spatially and temporally (e.g., Figure 1b,c), while artificially planted dunes often have even sparser vegetation (e.g., Figure 1d). To characterize the range of potential dune grass configurations, as observed from field data from White and described in Section 2.1, additional representations of vegetation in the model were included. First, uniform ρ_{veg} grids of 10%, 50%, and 90% were generated to represent a range from low vegetation density cases that might be representative of recent planting of dune grass sprigs ($\rho_{veg} = 10\%$), to a mature dune system where grass has reached high densities ($\rho_{veg} = 90\%$). Each of the 63 morphologic simulations were repeated with these new, uniform, 10%, 50%, and 90% ρ_{veg} grids.

Beyond these initial vegetation model runs, in which vegetation density is constant across the dune face, we included additional cases simulating non-uniform gradients in ρ_{veg} to more accurately replicate real-world conditions in which dune vegetation is spatially gradational. Statistical analysis of ecological data from northern Outer Banks dunes [19] found a median dune crest ρ_{veg} value of 35% (SD = 22%). Gradient cases assume a local ρ_{veg} of 0% at z_{toe} that linearly increases to ρ_{veg} of 35% at the dune crest and any location landward of the crest (Figure 4). Recognizing that the 35% ρ_{veg} value is a median, and that there is wide variability in dune ecological characteristics in the region of interest, the same gradient methodology was repeated for one standard deviation above ($\rho_{veg} = 67\%$) and below ($\rho_{veg} = 3\%$) the median-value dune crest ρ_{veg} (i.e., 35%). Similar cross-shore gradients in ρ_{veg} were established for each case, and each run for all 63 morphologies. Together, these seven ecological configurations (10%, 30%, 50%, and 90% uniform ρ_{veg} , and 3%, 35%, and 67% gradient ρ_{veg}) resulted in 441 different cases run under the 2019 (modern) environmental time series.

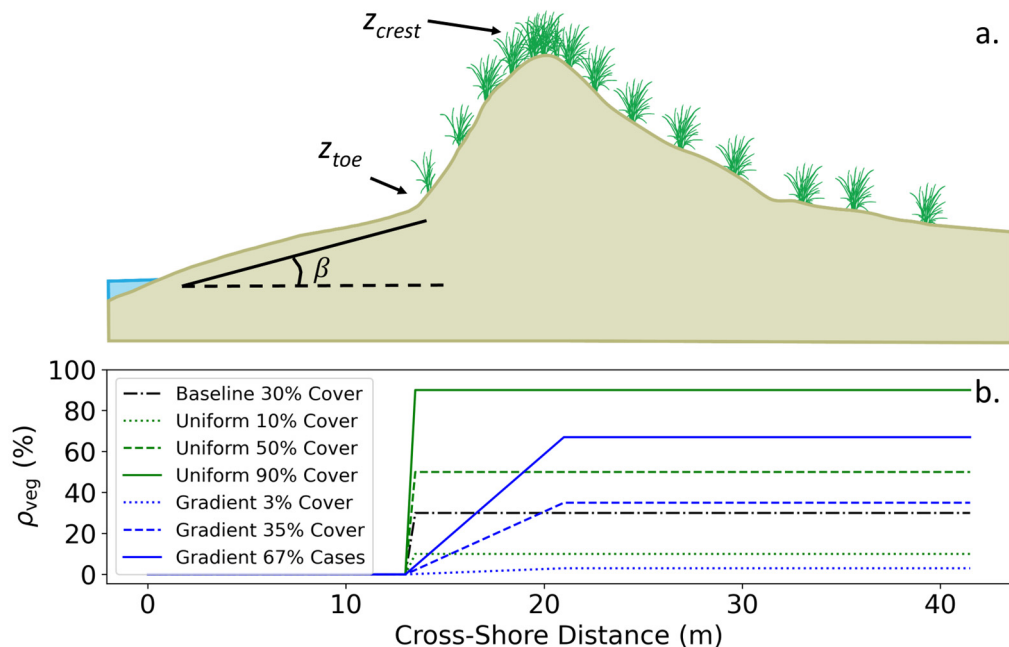


Figure 4. (a) Conceptual model of increasing vegetation cover across the dune face and (b) implementation of the various cases of spatially uniform and cross-shore gradient ρ_{veg} .

2.3.3. Exploratory Climate Change Scenarios

Lastly, to better constrain how time-evolving environmental conditions may alter dune morphodynamics, additional simulations were conducted in which we modified the 2019 (modern baseline) environmental time series. Specifically, to assess possible changes in storminess, the approach of Santos et al. [6] was implemented to modify the strength of storm events. All energetic wave events were first selected based on a criterion of daily peak significant wave height. The maximum wave height, SWL, and wind speed for each such event were increased by 5% to mimic a possible future climatic response that includes some amplification of storm characteristics. A triangular function was used to taper these 5% increases to the baseline conditions 6 h before and after the peak conditions. An example of these changes for a single storm are shown in Figure 2f,g. The 5% storminess increase was paired with a 0.5 m SLR increase to represent a possible environmental state experienced by these dunes in the future. In this case, a uniform 0.5 m increase was added to the SWL time series input to AeoliS. All the aforementioned morphologic and ecological conditions were re-run for the low-end climate change condition, henceforth referred to as the low-risk scenario. An additional, more extreme, possible climate change case was included that also increased the storminess by 5% but instead used a 1.5 m increase in sea level, henceforth referred to as the high-risk scenario.

2.4. Model Outputs

During AeoliS model simulations, data were stored in a netCDF file every 1 model hour, with each of our model runs totaling 1 year. Post-processing steps included interpolating cases presenting model instabilities (6 simulations across all 1323 model runs), calculating dune volume change, comparing pre- and post-model dune profiles, and contrasting the normalized deposition distance and height for each vegetation pattern. Dune volume change (ΔV_{dune}) was based on the difference in pre- and post-run dune profile elevation (z) above the toe elevation (z_{toe}), calculated across the center alongshore grid. The maximum deposition distance and height for each run were first normalized against the baseline case simulations and then averaged across the respective vegetation pattern.

3. Results

3.1. Baseline Case

The AeLoLiS model was used to simulate profile evolution at an annual scale, with morphologic responses dependent upon both the environmental conditions and initial morphology. Under the 2019 offshore environmental time series, the 63 different combinations of dune toe elevations and beach slopes resulted in ΔV_{dune} ranging from $+5.5 \text{ m}^3/\text{m}$ to $-71.1 \text{ m}^3/\text{m}$ over the year-long simulation (Figure 5a). Under modern-day conditions, dunes with lower toe elevations and steeper beach slopes experienced more erosion than dunes with high toe elevations and gentle beach slopes (Figure 6b). For example, a profile with a higher dune toe elevation ($z_{\text{toe}} = 4 \text{ m}$), fronting a relatively steep beach ($\tan\beta = 0.2 \text{ m/m}$), experienced the greatest degree of erosion, while a lower dune toe and shallower beach slope ($z_{\text{toe}} = 2.5 \text{ m}; \tan\beta = 0.075 \text{ m/m}$) resulted in the highest accretion among the set of simulated baseline scenarios. Approximately 65% of the morphological pairs of z_{toe} and $\tan\beta$ simulated for these baseline cases yielded net dune accretion (Figure 6). These accretional dunes exhibited a range of morphologic responses depending on the total volumetric change experienced at the annual scale, which was largely controlled by the relative contribution of marine (scarping and retreat) and aeolian (dune growth) processes aggregated across the simulation. Numerous simulations that resulted in scarping due to wave collision with the dune face also showed net total dune growth. This was associated with wind-driven sediment accumulation on the upper portion of the dune that compensated for losses along the marine margin. A subset of the scenarios that had high dune toe elevations and/or gentle beach slopes did not experience erosion events and only experienced accretion.

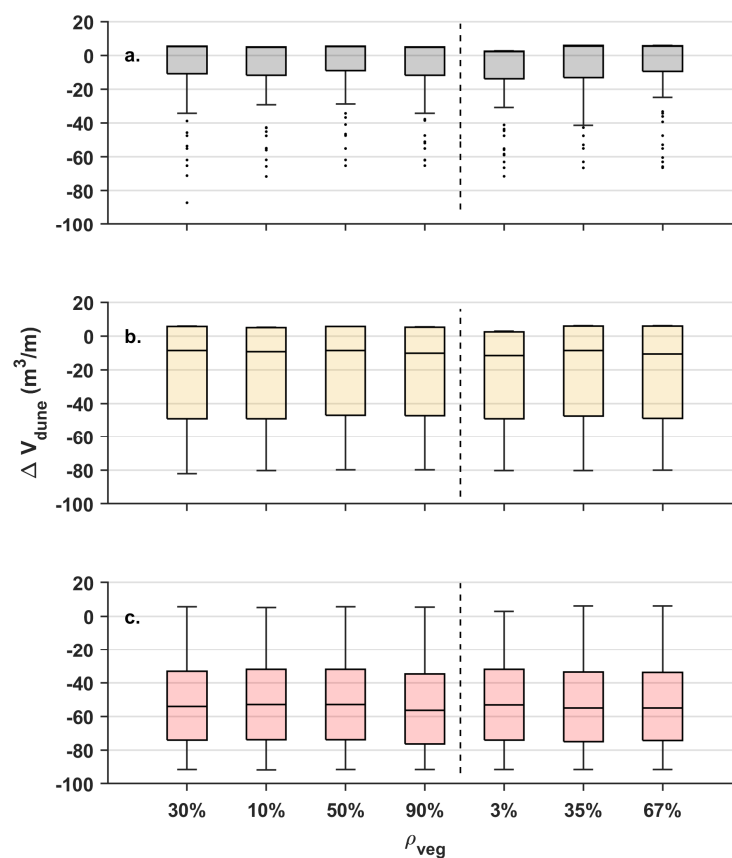


Figure 5. Range of net annual dune volume change (ΔV_{dune}) for all uniform (left of dashed line) and gradient (right of dashed line) vegetation scenarios under: (a) modern-day conditions, (b) low-risk climate change conditions, and (c) high-risk climate change conditions. Negative values indicate net loss of volume.

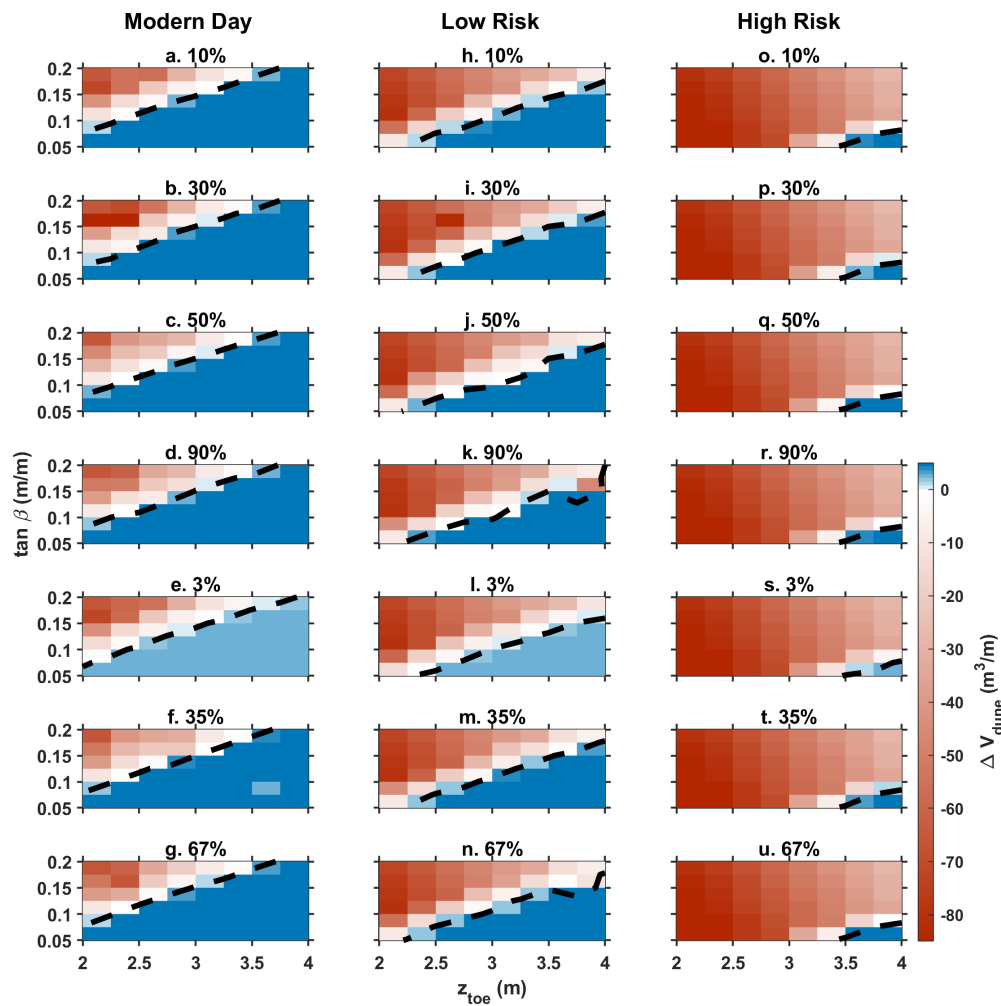


Figure 6. Simulated annual dune volume change (ΔV_{dune}) for various combinations of dune toe elevations (z_{toe}) and beach slopes ($\tan \beta$) with varying ρ_{veg} after modern-day climate (a–g), low-risk climate (h–n), and high-risk climate (o–u).

3.2. Environmental Forcings

Incorporating potential climate change effects by modifying the environmental time series input into the model can lead to a considerable shift in the annual dune volume change. Dune volume change for the low-risk climate scenario ranged from $+5.7 \text{ m}^3/\text{m}$ to $-80.0 \text{ m}^3/\text{m}$, and for the high-risk climate scenario ranges from $+5.7 \text{ m}^3/\text{m}$ to $-91.6 \text{ m}^3/\text{m}$ (Figure 5b–c). For some morphologies (e.g., $z_{\text{toe}} = 3.5\text{--}4.0 \text{ m}$ and $\tan \beta = 0.05 \text{ m/m}$), increased storminess in conjunction with an increased sea level led to enhanced accretion (Figure 6i), as compared with modern-day conditions. Altering climate conditions largely led to a greater magnitude of net erosion associated with more frequent dune collision and scarping (Figures 5b,c and 7) and led to more morphologies experiencing net erosion (Figure 6h–u). The low-risk and high-risk climate conditions, respectively, more than doubled and tripled the percent of dune morphologies that are net erosional (Figure 6). Under the high-risk climate condition, most cases resulted in substantial dune volume losses and, in some cases, even erosion of the entire dune to the landward extent of the model domain (e.g., Figure 7).

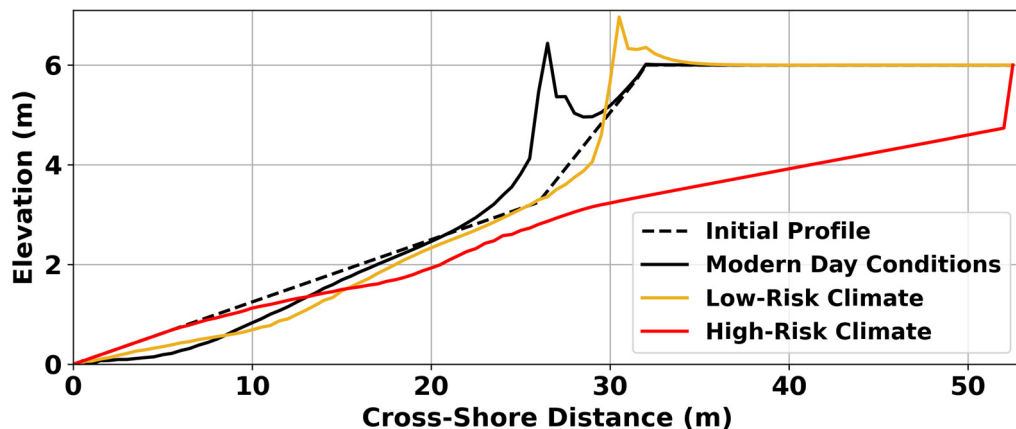


Figure 7. Example of initial and final cross-shore beach and dune profiles ($z_{toe} = 3.25$ and $\tan\beta = 0.125$).

3.3. Vegetation Influence

3.3.1. Uniform Vegetation Cover

Variable uniform vegetation densities showed little influence on the morphology cases run under all modeled climate conditions (Figures 5 and 6). Under modern-day conditions, dunes with 10%, 50%, and 90% ρ_{veg} experienced +5.0 to -71.6 , +5.5 to -65.3 , and +5.0 to $-65.2 \text{ m}^3/\text{m}$ of growth/erosion over the simulation period (Figure 5). These findings indicate that the medium (50%) ρ_{veg} case trapped the most sediment, whereas in the low-vegetation-density ($\rho_{veg} = 10\%$) scenario, more sediment was transported landward by wind (e.g., Figure 8a). In the high-vegetation-density ($\rho_{veg} = 90\%$) scenario, a substantial proportion of sediment was retained in the lower portion of the dune and subject to marine forcing (e.g., Figure 8a). In the case of large wave-driven erosion of the dunes, cases with the lowest values of ρ_{veg} lost the most sediment, whereas the model indicates that the 90% ρ_{veg} cases lost comparatively less sediment overall.

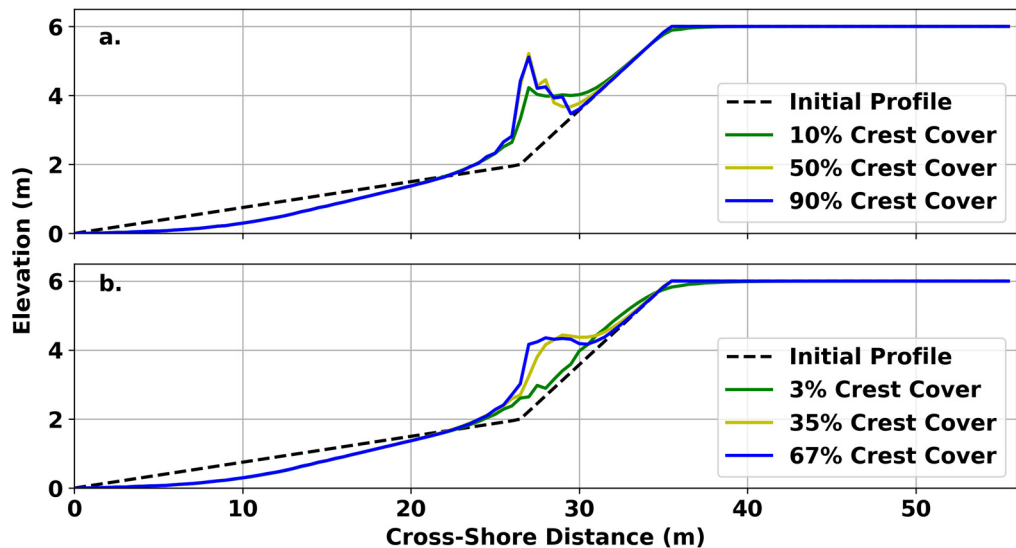


Figure 8. Example of net cross-shore profile evolution under modern-day conditions for different (a) uniform ρ_{veg} values and (b) lateral gradations in ρ_{veg} . Both profiles were run with $z_{toe} = 2 \text{ m}$ and $\tan\beta = 0.075 \text{ m/m}$.

Under low-risk conditions, dunes with 10%, 50%, and 90% ρ_{veg} experienced +5.2 to -80.3 , +5.6 to -79.9 , and +5.3 to $-79.9 \text{ m}^3/\text{m}$ of growth/erosion, while high-risk conditions led to ranges of +5.2 to -91.8 , +5.6 to -91.6 , and +5.3 to $-91.6 \text{ m}^3/\text{m}$. Though the altered climate conditions increased maximum net accretion, the overall percentage of net erosive

dunes doubled and tripled under low- and high-risk conditions (Figure 6). Regardless of climate state, dunes with 50% ρ_{veg} showed the most aggregation overall, as compared with 10% and 90% (Figures 5 and 9).

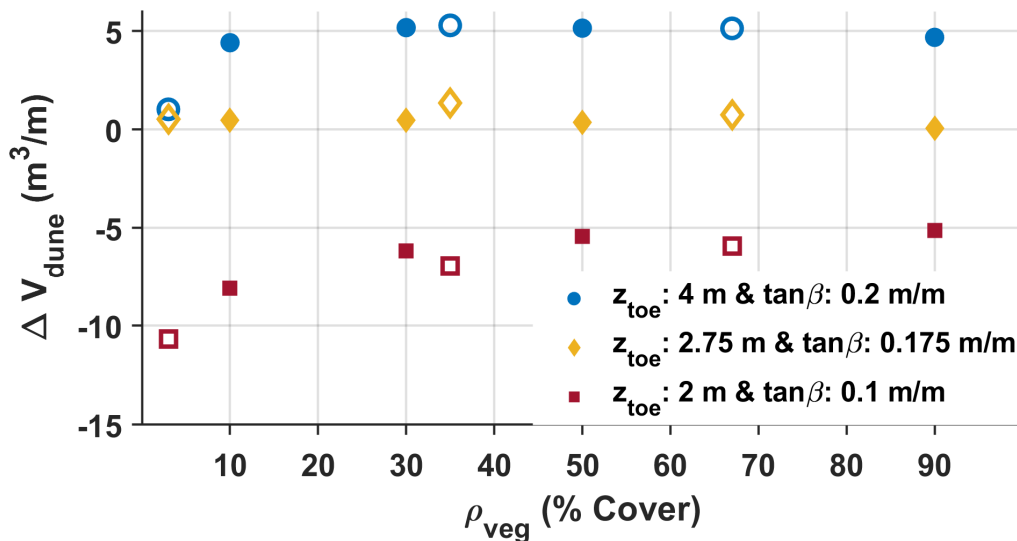


Figure 9. Example of modeled changes in dune volume under modern-day climate conditions for representative accretional (blue), erosional (red), and intermediate (yellow) morphologies with uniform (solid) and gradient (open) vegetation densities consistent across the dune slope.

3.3.2. Gradient Vegetation Cover

Modeled dunes incorporating vegetation gradients showed little variation from those with uniform vegetation cover. Similar to the uniform vegetation cases, the median ρ_{veg} value (35%) accumulated the most sediment (Figure 9). Under modern-day conditions, dunes with ρ_{veg} gradients of 3%, 35%, and 67% experienced dune volume changes of +2.7 to -71.5, +5.9 to -66.5, and +5.8 to -66.4 m³/m (Figure 5a). When crest ρ_{veg} = 3%, dunes with accretional morphologies experienced small amounts of aggregation across the whole dune face. In contrast, when crest ρ_{veg} = 35% and 67%, dunes with accretional morphologies aggraded the most sediment, but only at lower elevations (e.g., Figure 8b). Low-risk climate shifted the dune volume changes for dunes with the same ρ_{veg} to +2.8 to -80.3, +6.1 to -80.3, and +5.9 to -80.2 m³/m (Figure 5b), while high-risk conditions led to ranges of +2.8 to -91.7, +6.0 to -91.6, and +6.0 to -91.6 m³/m dune volume change (Figure 5c).

When all variable-vegetation cases were compared to the baseline morphology scenario under modern-day conditions, we found that the greatest differences were in those with lower dune toe elevation and steeper beach slopes (Figure 10). Under modern-day conditions, dunes with higher dune toes fronted by shallower-sloping beaches, with ρ_{veg} of uniform 50% and 90% and ρ_{veg} gradients of 35% and 67%, experienced a higher magnitude of deposition than the baseline case (Figure 10b,c,e,f). However, dunes with the same morphologies and ρ_{veg} of 10% (uniform) and 3% (gradient) displayed a lower magnitude of deposition than the baseline case (Figure 10a,d). Comparatively, differences in dune erosion/accretion for low-risk cases mostly deviated closer to the erosion/accretion threshold (Figure 10g–l).

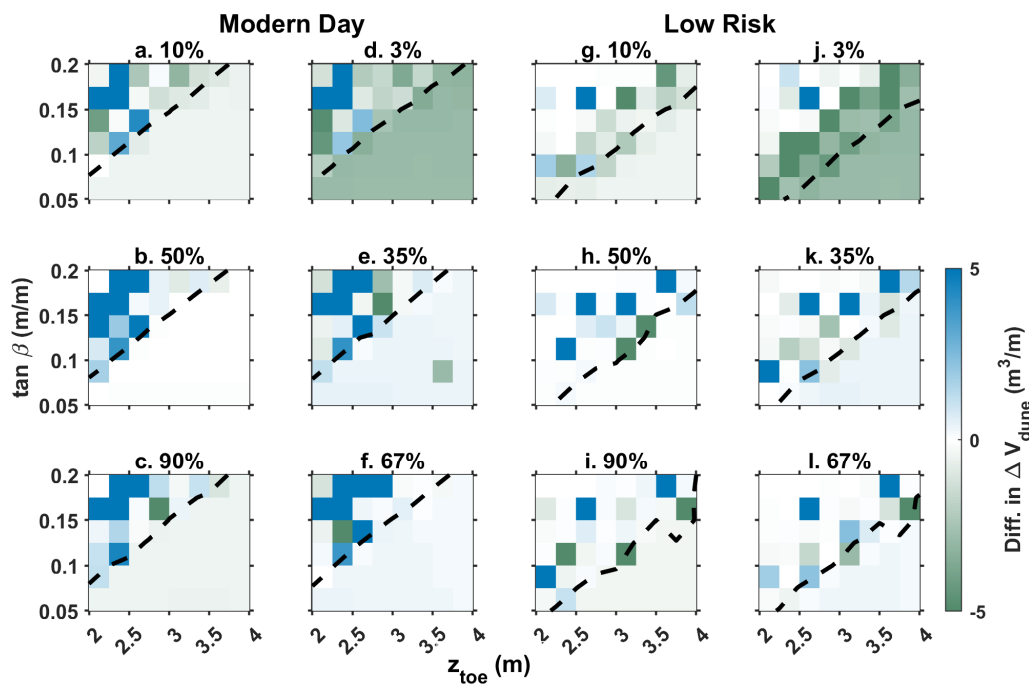


Figure 10. Differences in modeled dune volume changes ($\text{Diff. in } \Delta V_{\text{dune}}$) after the simulation period between baseline 30% ρ_{veg} and all uniform ρ_{veg} values (a–c,g–i) and gradient ρ_{veg} values (d–f,j–l) of vegetation cover for all combinations of beach and dune morphology. Dashed line shows the accretion/erosion threshold overlaid from Figure 6.

4. Discussion

4.1. Morphologic Controls

Dune erosion is typically influenced by the frequency and duration of exceedance of TWL over the dune toe elevation. This varies based on offshore wave conditions [15], dune toe elevation [52], beach width, and slope [11,53]. Dunes with higher toe elevations often experience decreased wave collision and, therefore, less erosion and loss of lower dune volume [14]. Beach width also imparts a primary control on dune erosion: wider beaches create a dissipative system, decreasing wave run-up and the resultant impact on the lower dune [15,53]. These general trends have also been observed at Duck, with sites of localized high rates of dune retreat often observed in areas with anomalously steep beaches, low dune toes, and/or deep offshore bathymetry [54].

Consistent with both the literature and local observations, the AeLoS model runs for the baseline, modern-day environmental forcings indicated that initial dune and beach morphology play an important role in annual dune volume changes (Figure 6). Simulated dunes with net accretive behavior are those fronted by beaches with a gentler beach slope, while dunes fronted by a steeper beach slope only experienced net annual erosion (Figure 6). Model results, which integrated both aeolian and marine processes, indicated that locations with steep beach slopes and low dune toe elevations are unlikely to maintain stable foredunes in the long term (decades) without active management to either rebuild dunes or add sediment to the beach. This may point to a rationale for why low-elevation dune toes (below 2.5 m) were rare in this study region; that is, they may reflect a transient morphologic state. These low dune toes are likely to naturally increase in elevation over time through avalanching of the scarped dune face and negative morphodynamic feedback that may serve to prevent runaway erosion. We found the potential volume losses from wave collision were much higher than the potential dune volume gains from wind-driven sediment transport processes (Figure 6) among the morphological conditions simulated. Thus, episodic erosion events could also serve to shallow beach slopes through rapid lateral retreat of the dune toe during major erosional storms and through transfer of some subset of those eroded dune sediments onto the beach.

Beach properties also play an active role in modifying aeolian dynamics in coastal systems. Wider beaches (generally those with shallower slopes) are unlikely to be fetch-limited in terms of transport saturation (e.g., [8]). Terrestrial lidar mapping of beach–dune systems found that beach slopes similarly play a role in controlling dune volume change in the United Kingdom [55] and the Netherlands [10]. In this present AeoliS application, modeled dune growth rates upward of $5 \text{ m}^3/\text{m/year}$ along sites with low-gradient beach slopes are consistent with field observations from the Outer Banks [45]. Interestingly, a relatively major storm, such as Hurricane Dorian (2019), was insufficient to drive substantial erosion for most combinations of beach slope and dune toe elevation, and in some cases resulted instead in dune accretion. Therefore, while dune growth rates may be modest at the annual scale, the aggregation of these sediment fluxes over a decade or longer, in the absence of any catastrophic collision events, can contribute to the growth of entirely new foredune systems, as has been observed at the FRF in recent years by Brodie et al. [43] and are common along progradational beach systems (e.g., [56]). This highlights the degree to which natural processes can aid dune resilience over time. This is particularly important to consider from a coastal management lens, considering that dune stability and growth are likely to be impacted under evolving climate conditions (e.g., Figures 6, 7, and 10).

4.2. Ecological Controls

The presence of vegetation is generally recognized from field studies as reducing wave-driven erosion [27,28]. Over short timescales (i.e., minutes), the density of vegetation can serve to reduce erosion [57]. While the influence of vegetation on dune collision dynamics was not included in our modeling framework, vegetation did play a role in modeled accretional dune eco-morphodynamics. Dune vegetation reduces wind velocity and allows sediment to fall out of suspension [31,58], thus amplifying aeolian deposition over time. Considering the inclusion of the Raupach et al. [48] equation into AeoliS, we expected dunes with higher vegetation cover to experience overall greater annual net accretion within the model simulations. We found an increase in accretion as uniform ρ_{veg} was changed from 10% to 50%, and as gradational ρ_{veg} increased from 3% to 35% (Figures 6, 8, and 10). However, our results indicated that intermediate vegetation densities (i.e., 50% and 35% ρ_{veg}) yielded the greatest net accretion over a single-year period under modern-day conditions (e.g., Figure 9), suggesting the existence of an idealized threshold of vegetation cover to promote dune growth.

Maximum accretion at intermediate densities may be explained by the modeled distribution of vegetation across the dune: in our model runs, the lowest elevation with vegetation present was located at the prescribed dune toe, encouraging accretion principally at the toe through vegetation-induced sediment trapping. In this vegetation distribution, sediment flux to the stoss slope and crest is subsequently hindered. Keijser et al. [59] observed a similar process, where maximum sedimentation occurred at the highest vegetation density (at lower elevations) and decreased landward. Figure 10b indicates that cases with the highest (90%) ρ_{veg} values resulted in 15% more aggradation at the zone of maximum deposition, relative to the 30% ρ_{veg} case. Conversely, a lower ρ_{veg} resulted in sediment spread over a wider cross-shore area and a lower maximum height of sediment deposition than a higher ρ_{veg} (Figure 11). These model results are consistent with field observations that have demonstrated that sparse dune vegetation allows more sand to be transported landward [60]. We overall found that vegetation gradient cases led to a greater distance of deposition from the dune toe (Figure 11a), while uniform vegetation cases led to a greater deposition height (Figure 11b).

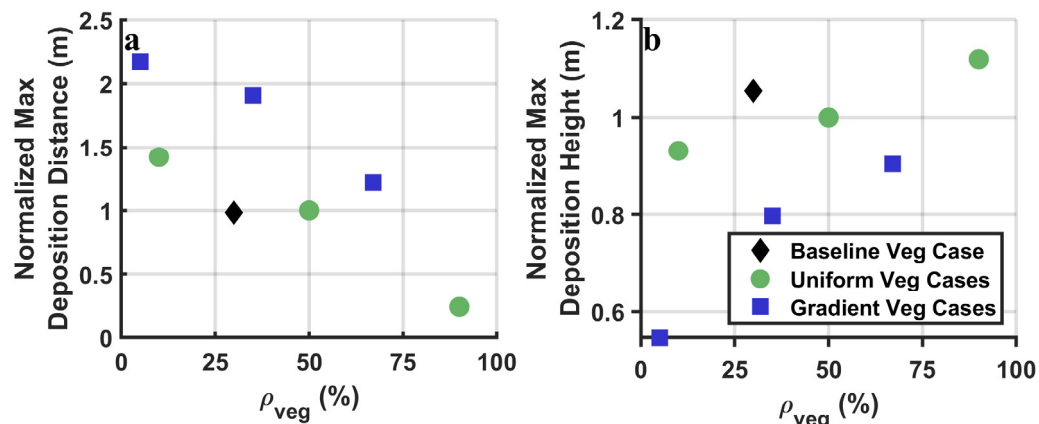


Figure 11. Respective (a) average maximum distance of deposition from the dune toe and (b) average maximum deposition height on the dune face of the 63 morphology combinations of each ρ_{veg} pattern (i.e., uniform 10%, 30%, 50%, and 90%, and gradient 3%, 35%, and 67%), normalized relative to the values for the baseline ($\rho_{veg} = 30\%$) case.

High ρ_{veg} at the dune toe served to concentrate sediment deposition at lower elevations (Figures 8 and 11a), where it could subsequently be eroded during elevated TWL events if TWLs exceeded the dune toe elevation. This concentrated zone of deposition near the beach–dune boundary contributed to the slightly lower rates of net dune volume change for many simulations relative to moderate ρ_{veg} cases, where sediment could be transported by wind further into the dune complex and was, therefore, not eroded during high-energy events. These aggregate results suggested that planting strategies could be optimized to either encourage (1) dune widening by facilitating a narrower zone of deposition near the dune toe, or (2) aggradation of the entire dune profile, thereby promoting dune heightening, through the use of sparser planting. Our results overall showed that dunes with a cross-shore gradient of vegetation with an intermediate density close to the dune crest may have the highest potential for annual progradation.

Our observation of lower rates of accretion on modeled dunes with high vegetation densities could also be explained by the default ecological parameterization of AeoliS. AeoliS assumes vegetation dies instantaneously after interacting with wave run-up; however, live vegetation can sustain some level of seawater inundation depending on the species. Because vegetation growth and expansion were turned off for these exploratory simulations, if storm surge occurred early in the simulation, the plants were no longer accounted for, negating any accretional capabilities contributing to dune rebound. Nonetheless, our results align with published dune manuals and guides encouraging planting of sparse vegetation at the dune toe and increasing vegetation densities closer to the dune crest and at higher elevations to optimize sediment trapping [61]. Additionally, Hesp et al. [26] demonstrated, with artificial vegetation and a wind tunnel, that deposition of wind-driven sediment does not necessarily occur at the immediate front of a vegetation patch. Using the wind experiments of Hesp et al. [26] and additional field measurements from the Oregon, USA coast, Dickey et al. [25] also showed that using a far-field vegetation shear coupler improved the simulation of deposition patterns relative to the approach of Raupach et al. [48] in coastal dune fields with sparse vegetation. Incorporating any far-field deposition effects from both dense and sparse vegetation into the results of this present study could translate sediment deposition even further into the dune complex and similarly reduce the likelihood of wave-driven erosion of those sediments. While vegetation is an effective agent for sediment trapping under modern conditions, climatic changes are likely to shift dune systems toward net erosion under a broader set of morphological conditions (e.g., Figure 6).

4.3. Future Dune Vulnerability under Variable Environmental Forcings

Future climate changes are likely to lead to enhanced coastal hazards, including increased storm surge, flooding, and beach erosion, resulting from the combined forces of rising sea levels and increased storminess. Incorporation of multiple forcings into numerical models is needed to gain realistic projections of coastal change and help identify evolving best management practices (e.g., [62]). For example, higher background water levels amplify storm surge and will result in wave run-up exceeding the dune toe more frequently, leading to an increase in the duration and magnitude of wave-driven dune erosion [63]. Simultaneously, higher TWLs decrease aeolian transport of beach sand by reducing the area of dry, exposed sediment available for transport, which ultimately reduces wind-driven sediment inputs to the dune [64].

The instantaneous increase in SWL applied in our models did not fully capture the intricacies of coastal change associated with a gradual rise in SLR. Further, many uncertainties remain regarding the nature of how storm patterns will shift in the future [3], which cannot be accounted for in our approach. Nonetheless, this numerical modeling approach does allow for an assessment of (1) hypothetical scenarios and (2) insight into potential challenges in maintaining the status quo of dune resilience even a short time into the future, while trying to maintain the current seaward extent of the shoreline.

In our simulations, the number of beach and dune morphology combinations that experienced net accretion decreased by 20–25% under low-risk climate conditions and further decreased by 30–37% under high-risk climate conditions, relative to the baseline (modern) conditions. However, in the low-risk scenario, dunes with the highest toe elevations and fronted by dissipative beach slopes showed a slight increase in modeled accretion for both climate scenarios (Figures 5 and 6), reflecting the possible positive contribution of increased storminess to dune accretion through increased aeolian activity driven by higher peak wind velocities during energetic storms. Considering that foredunes along developed coasts generally cannot migrate landward [65], these added wind-driven sediment fluxes under future climate forcings may help to offset some losses associated with more extreme marine forcings (i.e., wave erosion) in the future. Whether a particular dune experiences accretion or erosion during a specific event can be highly dependent on sub-tidal sequencing of tides, peak storm surge, peak wave characteristics, and peak wind characteristics, complicating our ability to associate any single instance of aeolian, storm-driven dune growth with climate change.

We found that the threshold for net accretional versus erosional conditions (dashed black line in Figure 6 subpanels) shifted toward higher dune toe elevations and gentler beach slopes for both low-risk and high-risk climates. In other words, more combinations of beach and dune morphologies will be vulnerable to erosion under modeled climate conditions. The percentage of beach and dune morphology combinations experiencing erosion shifted from ~35% under modern-day conditions to ~60% under low-risk conditions, and to ~90% for high-risk conditions (Figure 6). This indicates that the accretional abilities of increased storminess did not offset subsequent erosion caused by elevated background TWLs from higher SLR for the vast majority of beach and dune morphologies found along the northern North Carolina Outer Banks. Our model results indicate that a wider variety of dune morphologies are susceptible to erosion when subjected to compound effects of higher SLR and increased storm intensity (high-risk climate scenario; Figure 6). Dunes in the modeled high-risk climate also experienced a greater magnitude of erosion. Considering the singular difference between low- and high-risk conditions is the SLR scenario, SLR may be a more predominant environmental forcing with regard to dune volume loss, as compared to enhanced storminess, in the coming century. This finding is consistent with Ranasinghe et al. [66], who used a multi-scale Probabilistic Coastline Recession model to determine the relative impact of SLR and storm erosion on sandy coastlines.

Increases in both sea level and storminess led to greater variation in volume change for dunes fronted by gently sloping beaches, while dunes fronted by steeper beaches showed similar volume losses between modern-day and altered climatic conditions (Figure 6). This

unexpected result may reflect the predisposed vulnerability of dunes fronted by steeper beaches to overtopping under modern-day conditions [15], or the decreased opportunity for wave-energy dissipation while traveling up steeper beaches [67]. In the coming decades and century, we will likely see decreased annual dune stability (and accelerated erosion) along beach–dune systems with attributes similar to those in the northern North Carolina Outer Banks.

4.4. Numerical Approach

Previous approaches to modeling dune evolution at annual scales have either neglected erosive marine processes (e.g., [35,56]) or attempted to fully simulate feedback between the subaqueous and subaerial zones using coupled modeling tools (e.g., [29]). This model effectively pairs the process-based aeolian sediment transport model AeoliS [35] with a dune-erosion module derived from Palmsten and Holman [14]. AeoliS was used to efficiently simulate annual-scale dune evolution on timescales of minutes to hours, as compared with models requiring high computational power and large amounts of time to complete simulations (e.g., XBeach–Duna and Windsurf).

It is important to note that this model application makes assumptions that limit its realistic representation of real-world dune processes, including defining beach and dune shapes by an initial planar morphology and simplifying vegetation–sediment interactions, accounting for only a single species. Vegetation effects on marine processes were also not directly included in the modeling exercises presented here; however, incorporation of the *in situ* shear strength of the vegetated dune into the dune erosion solver (following methods of Ajedegba et al. [68]) could allow for this additional morphodynamic feedback to be resolved. Ongoing work is also being carried out to couple AeoliS with DOONIES [69], a photosynthesis-based ecological model developed for coastal settings, to create a more comprehensive tool to study short-term coastal dune evolution, including dynamic vegetation growth and expansion effects.

Furthermore, our methodology assumes a constant beach slope through time, and that dune collision always results in erosion (following the framework of Palmsten and Holman [14]), thus neglecting the possible role of swash deposition at the base of the dune. Our approach to modifying meteorological and oceanographic forcings by fixed percentages for TWL over 3 m is also likely overly simplistic: global climate models typically include rigorous statistical analyses, incorporation of storm climatology, and detailed offshore hydrodynamical modeling, all of which this methodology lacks [70]. Our climate assumptions, along with inherent limitations in process-based morphodynamic models in representing the full suite of real-world physical processes acting on dune–beach systems, should be considered when interpreting the model results.

Nevertheless, our approach is illustrative of potential changes to the state of dune systems under broadly more energetic conditions. We stress that the primary aeolian and marine drivers of coastal foredune change are included in AeoliS, and that these results can, therefore, provide valuable insights into the potential ecomorphodynamic controls on present and future dune evolution. Additional work is needed to understand the long-term combined effects of changing static (sea level) and dynamic (winds, waves, and surge) environmental conditions on dune processes at multidecadal to centennial timescales. Further modeling should also be performed to assess the potential offset of dune volume change under climate conditions for varying management strategies. Possibilities include varying vegetation species within the model, introducing sand fences, or varying the beach width to represent (for example) artificial beach nourishment, along with detailed validation of these behaviors against field data.

5. Conclusions

This study used numerical modeling to investigate potential shifts in erosional versus accretional behavior of coastal dunes in response to ecological spatial variability and changing climate conditions. The results indicated that annual dune evolution is highly

dependent on the pre-existing morphology of the beach and dune. Consistent with field observations, we found that the most resilient dunes were those characterized by high-elevation dune toes, fronted by shallow-sloping beaches, and with a cross-shore gradient of vegetation with an intermediate density close to the dune crest. Sites with shallow-sloping beaches and/or higher dune toe elevations are likely to be less vulnerable to dune erosion and more likely to experience dune growth from aeolian inputs, as compared with steeper beaches and/or lower-elevation dune toes, even under high-risk climate scenarios. As such, we found that dunes with low toe elevations fronted by steep beaches were the most vulnerable to changes in environmental conditions. Furthermore, the resilience of dunes with high toe elevations fronted by gentle sloping beaches can be improved by dune vegetation distribution changes more than dunes with low toe elevations fronted by steep beaches because of their predisposed accretional capabilities. Under all altered climate conditions, our modeling revealed that, while dune vegetation can enhance dune growth, the precise vegetation strategies (e.g., spatially varying planting densities) play the primary role in the spatial distribution of sediment deposition. For example, planting vegetation gradients could lead to more sediment deposition across the dune face, while planting uniform vegetation may lead to more deposition at the dune toe. These results show how even exploratory numerical models can inform or optimize coastal management actions, such as assessing tradeoffs for different dune designs or planting strategies.

Author Contributions: Conceptualization, S.S.H., N.C., E.H.D. and C.J.H.; methodology, S.S.H., N.C., E.H.D., A.W., C.J.H. and J.C.Z.; software, N.C.; formal analysis, S.S.H. and N.C.; investigation, S.S.H. and N.C.; resources, N.C. and C.J.H.; data curation, S.S.H. and N.C.; writing—original draft preparation, S.S.H., N.C., E.H.D. and A.W.; writing—review and editing, S.S.H., N.C., E.H.D., A.W., C.J.H. and J.C.Z.; visualization, S.S.H.; supervision, N.C. and C.J.H.; project administration, N.C., C.J.H. and J.C.Z.; funding acquisition, N.C., C.J.H. and J.C.Z. All authors have read and agreed to the published version of the manuscript.

Funding: This work was funded by NOAA’s National Centers for Coastal Ocean Science, Effects of Sea Level Rise (ESLR) Competitive Research Program, under award NA19NOS4780175, the US Army Engineer Research and Development Center’s (ERDC) Coastal Inlets Research Program (CIRP) base program, and the ERDC Coastal Forecasting to Reduce Infrastructure Flooding (CFRIF) program.

Institutional Review Board Statement: Not applicable.

Informed Consent Statement: Not applicable.

Data Availability Statement: Wave and wind data used to force the model were sourced from the US-ACE Wave Information Studies Database (<https://wisportal.erdc.dren.mil/>, accessed on 1 June 2022). Tide time series from the Duck, NC FRF Pier, were downloaded from the NOAA Tides and Currents database (<https://tidesandcurrents.noaa.gov/>, accessed on 1 June 2022). Version 2.1.1 of the open-source AeoliS model (<https://github.com/openearth/aeolis-python>, accessed on 1 September 2023) was used in this application, which can be downloaded via PyPI (<https://pypi.org/project/aeolis/2.1.1/>, accessed on 1 June 2022).

Acknowledgments: We thank Janelle Skaden for initial help with AeoliS model setup scripts. This research was supported in part by an appointment to the Department of Defense (DOD) Research Participation Program administered by the Oak Ridge Institute for Science and Education (ORISE) through an interagency agreement between the US Department of Energy (DOE) and the DOD. ORISE is managed by ORAU under DOE contract number DE-SC0014664. All opinions expressed in this paper are the authors’ and do not necessarily reflect the policies and views of the DOD, DOE, or ORAU/ORISE. This work is a contribution to IGCP Project 725 ‘Forecasting Coastal Change’.

Conflicts of Interest: The authors declare no conflicts of interest. The funders had no role in the design of the study; in the collection, analysis, or interpretation of data; in the writing of the manuscript, or in the decision to publish the results.

References

1. Marsooli, R.; Lin, N.; Emanuel, K.; Feng, K. Climate Change Exacerbates Hurricane Flood Hazards along US Atlantic and Gulf Coasts in Spatially Varying Patterns. *Nat. Commun.* **2019**, *10*, 3785. [[CrossRef](#)] [[PubMed](#)]
2. Sweet, W.V.; Hamlington, B.D.; Kopp, R.E.; Weaver, C.P.; Barnard, P.L.; Bekaert, D.; Brooks, W.; Craghan, M.; Dusek, G.; Frederikse, T.; et al. *Global and Regional Sea Level Rise Scenarios for the United States: Updated Mean Projections and Extreme Water Level Probabilities along U.S. Coastlines*; National Oceanic and Atmosphere Administration, National Ocean Service: Silver Spring, MD, USA, 2022.
3. Knutson, T.R.; Chung, M.V.; Vecchi, G.; Sun, J.; Hsieh, T.-L.; Smith, A.J.P. ScienceBrief Review: Climate Change Is Probably Increasing the Intensity of Tropical Cyclones. In *Critical Issues in Climate Change Science*; le Quéré, C., Liss, P., Forster, P., Eds.; 2021; CERN: Meyrin, Switzerland; pp. 1–8. [[CrossRef](#)]
4. Singhvi, A.; Luijendijk, A.P.; Van Oudenoven, A.P.E. The Grey—Green Spectrum: A Review of Coastal Protection Interventions. *J. Environ. Manag.* **2022**, *311*, 114824. [[CrossRef](#)] [[PubMed](#)]
5. Elko, N.; Brodie, K.; Stockdon, H.; Nordstrom, K.; Houser, C.; McKenna, K.; Moore, L.; Rosati, J.; Ruggiero, P.; Thuman, R.; et al. Dune Management Challenges on Developed Coasts. *Shore Beach* **2016**, *84*, 15–28.
6. Santos, V.M.; Wahl, T.; Long, J.W.; Passeri, D.L.; Plant, N.G. Combining Numerical and Statistical Models to Predict Storm-Induced Dune Erosion. *JGR Earth Surf.* **2019**, *124*, 1817–1834. [[CrossRef](#)]
7. Strypsteen, G.; Houhuys, R.; Rauwoens, P. Dune Volume Changes at Decadal Timescales and Its Relation with Potential Aeolian Transport. *JMSE* **2019**, *7*, 357. [[CrossRef](#)]
8. Delgado-Fernandez, I. A Review of the Application of the Fetch Effect to Modelling Sand Supply to Coastal Foredunes. *Aeolian Res.* **2010**, *2*, 61–70. [[CrossRef](#)]
9. Davidson-Arnott, R.G.D.; Law, M.N. Seasonal Patterns and Controls on Sediment Supply to Coastal Foredunes, Long Point, Lake Erie. In *Coastal Dunes: Form and Process*; John Wiley & Sons Ltd.: Hoboken, NJ, USA, 1990; pp. 177–200.
10. Silva, F.G.; Wijnberg, K.M.; de Groot, A.V.; Hulscher, S.J.M.H. The Effects of Beach Width Variability on Coastal Dune Development at Decadal Scales. *Geomorphology* **2019**, *329*, 58–69. [[CrossRef](#)]
11. Itzkin, M.; Moore, L.J.; Ruggiero, P.; Hacker, S.D.; Biel, R.G. The Relative Influence of Dune Aspect Ratio and Beach Width on Dune Erosion as a Function of Storm Duration and Surge Level. *Earth Surf. Dynam.* **2021**, *9*, 1223–1237. [[CrossRef](#)]
12. Mull, J.M. Coastal Sand Dunes in the U.S. Pacific Northwest: Regional Variability in Foredune Geomorphology and Associated Physical Vulnerability to Hazards. Master’s Thesis, Oregon State University, Corvallis, OR, USA, 2010.
13. Héquette, A.; Ruz, M.-H.; Zemmour, A.; Marin, D.; Cartier, A.; Sipka, V. Alongshore Variability in Coastal Dune Erosion and Post-Storm Recovery, Northern Coast of France. *J. Coast. Res.* **2019**, *88*, 25. [[CrossRef](#)]
14. Palmsten, M.L.; Holman, R.A. Laboratory Investigation of Dune Erosion Using Stereo Video. *Coast. Eng.* **2012**, *60*, 123–135. [[CrossRef](#)]
15. Stockdon, H.F.; Holman, R.A.; Howd, P.A.; Sallenger, A.H. Empirical Parameterization of Setup, Swash, and Runup. *Coast. Eng.* **2006**, *53*, 573–588. [[CrossRef](#)]
16. Larson, M.; Erikson, L.; Hanson, H. An Analytical Model to Predict Dune Erosion Due to Wave Impact. *Coast. Eng.* **2004**, *51*, 675–696. [[CrossRef](#)]
17. Wahl, T.; Plant, N.G.; Long, J.W. Probabilistic Assessment of Erosion and Flooding Risk in the Northern Gulf of Mexico. *JGR Ocean.* **2016**, *121*, 3029–3043. [[CrossRef](#)]
18. Konlechner, T.M.; Hilton, M.J. Post-disturbance Evolution of a Prograded Foredune Barrier during a Sustained Dynamic Restoration Project—The Role of Wind Speed, Wind Direction and Vegetation. *Earth Surf. Process. Landf.* **2022**, *47*, 3435–3452. [[CrossRef](#)]
19. White, A.E. Biotic Characteristics of Managed and Unmanaged Coastal Dunes in the Outer Banks, North Carolina. Master’s Thesis, Virginia Commonwealth University, Richmond, VA, USA, 2022.
20. McGuirk, M.T.; Kennedy, D.M.; Konlechner, T. The Role of Vegetation in Incipient Dune and Foredune Development and Morphology: A Review. *J. Coast. Res.* **2022**, *38*, 414–428. [[CrossRef](#)]
21. Ruggiero, P.; Hacker, S.; Seabloom, E.; Zarnetske, P. The Role of Vegetation in Determining Dune Morphology, Exposure to Sea-Level Rise, and Storm-Induced Coastal Hazards: A U.S. Pacific Northwest Perspective. In *Barrier Dynamics and Response to Changing Climate*; Moore, L.J., Murray, A.B., Eds.; Springer International Publishing: Cham, Switzerland, 2018; pp. 337–361. ISBN 978-3-319-68084-2.
22. Valentini, E.; Taramelli, A.; Cappucci, S.; Filippioni, F.; Nguyen Xuan, A. Exploring the Dunes: The Correlations between Vegetation Cover Pattern and Morphology for Sediment Retention Assessment Using Airborne Multisensor Acquisition. *Remote Sens.* **2020**, *12*, 1229. [[CrossRef](#)]
23. Charbonneau, B.R.; Dohner, S.M.; Wnek, J.P.; Barber, D.; Zarnetske, P.; Casper, B.B. Vegetation Effects on Coastal Foredune Initiation: Wind Tunnel Experiments and Field Validation for Three Dune-Building Plants. *Geomorphology* **2021**, *378*, 107594. [[CrossRef](#)]
24. Derijckere, J.; Strypsteen, G.; Rauwoens, P. Early-Stage Development of an Artificial Dune with Varying Plant Density and Distribution. *Geomorphology* **2023**, *437*, 108806. [[CrossRef](#)]
25. Dickey, J.; Wengrove, M.; Cohn, N.; Ruggiero, P.; Hacker, S.D. Observations and Modeling of Shear Stress Reduction and Sediment Flux within Sparse Dune Grass Canopies on Managed Coastal Dunes. *Earth Surf. Process. Landf.* **2023**, *48*, 907–922. [[CrossRef](#)]

26. Hesp, P.A.; Dong, Y.; Cheng, H.; Booth, J.L. Wind Flow and Sedimentation in Artificial Vegetation: Field and Wind Tunnel Experiments. *Geomorphology* **2019**, *337*, 165–182. [[CrossRef](#)]
27. de Battisti, D.; Griffin, J.N. Below-Ground Biomass of Plants, with a Key Contribution of Buried Shoots, Increases Foredune Resistance to Wave Swash. *Ann. Bot.* **2019**, *125*, mcz125. [[CrossRef](#)] [[PubMed](#)]
28. Feagin, R.A.; Furman, M.; Salgado, K.; Martinez, M.L.; Innocenti, R.A.; Eubanks, K.; Figlus, J.; Huff, T.P.; Sigren, J.; Silva, R. The Role of Beach and Sand Dune Vegetation in Mediating Wave Run up Erosion. *Estuar. Coast. Shelf. Sci.* **2019**, *219*, 97–106. [[CrossRef](#)]
29. Roelvink, D.; Costas, S. Coupling Nearshore and Aeolian Processes: XBeach and Duna Process-Based Models. *Environ. Model Softw.* **2019**, *115*, 98–112. [[CrossRef](#)]
30. Robin, N.; Billy, J.; Castelle, B.; Hesp, P.; Nicolae Lerma, A.; Laporte-Fauret, Q.; Marieu, V.; Rosebery, D.; Bujan, S.; Destribats, B.; et al. 150 Years of Foredune Initiation and Evolution Driven by Human and Natural Processes. *Geomorphology* **2021**, *374*, 107516. [[CrossRef](#)]
31. Wootton, L.; Miller, J.; Miller, C.; Peek, M.; Williams, A.; Rowe, P. Dune Manual 2016. Available online: <https://njseagrant.org/wp-content/uploads/2016/12/Dune-Manual-Pgs-for-website.pdf> (accessed on 1 May 2022).
32. Town of Duck Shore Protection Project: Beach Maintenance Plan 2020. Available online: https://www.townofduck.com/wp-content/uploads/DUCK-FEMA-Maintenance-Plan_Updated-2020.pdf (accessed on 1 May 2022).
33. Houser, C.; Wernette, P.; Rentschlar, E.; Jones, H.; Hammond, B.; Trimble, S. Post-Storm Beach and Dune Recovery: Implications for Barrier Island Resilience. *Geomorphology* **2015**, *234*, 54–63. [[CrossRef](#)]
34. Durán, O.; Moore, L.J. Vegetation Controls on the Maximum Size of Coastal Dunes. *Proc. Natl. Acad. Sci. USA* **2013**, *110*, 17217–17222. [[CrossRef](#)] [[PubMed](#)]
35. Hoonhout, B.M.; de Vries, S. A Process-based Model for Aeolian Sediment Transport and Spatiotemporal Varying Sediment Availability. *JGR Earth Surf.* **2016**, *121*, 1555–1575. [[CrossRef](#)]
36. Keijser, J.G.S.; De Groot, A.V.; Riksen, M.J.P.M. Modeling the Biogeomorphic Evolution of Coastal Dunes in Response to Climate Change: Modeling Coastal Dunes. *J. Geophys. Res. Earth Surf.* **2016**, *121*, 1161–1181. [[CrossRef](#)]
37. van IJzendoorn, C.O.; Hallin, C.; Reniers, A.J.H.M.; de Vries, S. Modeling Multi-Fraction Coastal Aeolian Sediment Transport with Horizontal and Vertical Grain-Size Variability. *JGR Earth Surf.* **2023**, *128*, e2023JF007155. [[CrossRef](#)]
38. van Westen, B.; de Vries, S.; Reniers, A.J.H.M.; den Bieman, J.P.; Hoonhout, B.M.; Rauwoens, P.; van Puijenbroek, M.E.B. Aeolian Modelling of Coastal Landform Development. In Proceedings of the Coastal Sediments 2019, St. Petersburg, FL, USA, 27–31 May 2019; World Scientific: Tampa/St. Petersburg, FL, USA, 2019; pp. 1354–1364.
39. Strypsteen, G.; de Vries, S. Simulating Profile Development of New Artificial Dune with Planted Vegetation for Sand Nuisance Mitigation. In Proceedings of the Coastal Sediments 2023, New Orleans, LA, 11–15 April 2023; World Scientific: New Orleans, LA, USA, 2023; pp. 732–738.
40. Birkemeier, W.A. Field Data on Seaward Limit of Profile Change. *J. Waterw. Port. Coast. Ocean Eng.* **1985**, *111*, 598–602. [[CrossRef](#)]
41. Dolan, R.; Davis, R.E. An Intensity Scale for Atlantic Coast Northeast Storms. *J. Coast. Res.* **1992**, *8*, 840–853.
42. Armstrong, S.B.; Lazarus, E.D. Masked Shoreline Erosion at Large Spatial Scales as a Collective Effect of Beach Nourishment. *Earth's Future* **2019**, *7*, 74–84. [[CrossRef](#)]
43. Brodie, K.; Conery, I.; Cohn, N.; Spore, N.; Palmsten, M. Spatial Variability of Coastal Foredune Evolution, Part A: Timescales of Months to Years. *JMSE* **2019**, *7*, 124. [[CrossRef](#)]
44. Jay, K.R.; Hacker, S.D.; Hovenga, P.A.; Moore, L.J.; Ruggiero, P. Sand Supply and Dune Grass Species Density Affect Foredune Shape along the US Central Atlantic Coast. *Ecosphere* **2022**, *13*, 2. [[CrossRef](#)]
45. Kaczkowski, H.L.; Kana, T.W.; Traynum, S.B.; Visser, R. Beach-Fill Equilibration and Dune Growth at Two Large-Scale Nourishment Sites. *Ocean Dyn.* **2018**, *68*, 1191–1206. [[CrossRef](#)]
46. Fenster, M.S.; Dolan, R. Historical Shoreline Trends along the Outer Banks, North Carolina: Processes and Responses. *J. Coast. Res.* **1993**, *9*, 172–188.
47. Cohn, N.; Brodie, K.L.; Johnson, B.; Palmsten, M.L. Hotspot Dune Erosion on an Intermediate Beach. *Coast. Eng.* **2021**, *170*, 103998. [[CrossRef](#)]
48. Raupach, M.R.; Gillette, D.A.; Leys, J.F. The Effect of Roughness Elements on Wind Erosion Threshold. *J. Geophys. Res. Atmos.* **1993**, *98*, 3023–3029. [[CrossRef](#)]
49. de Vries, S.; Hallin, C.; van IJzendoorn, C.; van Westen, B.; Cohn, N.; Strypsteen, G.; Skaden, J.; Agrawal, N.; Garcia Alvarez, M. 2023 AeoLiS (Version 2.1.1.) [Computer Software]. Available online: <https://github.com/openearth/aeolis-python> (accessed on 1 September 2023).
50. Brodie, K.L.; Spore, N.J. Foredune Classification and Storm Response: Automated Analysis of Terrestrial Lidar DEMs. In Proceedings of the Coastal Sediments 2015, San Diego, CA, USA, 11–15 May 2015; World Scientific: San Diego, CA, USA, 2015.
51. Inman, D.L.; Dolan, R. The Outer Banks of North Carolina: Budget of Sediment and Inlet Dynamics along a Migrating Barrier System. *J. Coast. Res.* **1989**, *5*, 193–237.
52. Splinter, K.D.; Kearney, E.T.; Turner, I.L. Drivers of Alongshore Variable Dune Erosion during a Storm Event: Observations and Modelling. *Coast. Eng.* **2018**, *131*, 31–41. [[CrossRef](#)]
53. Lemke, L.; Miller, J.K. Role of Storm Erosion Potential and Beach Morphology in Controlling Dune Erosion. *JMSE* **2021**, *9*, 1428. [[CrossRef](#)]

54. Conlin, M.P.; Cohn, N.; Adams, P.N. Total Water Level Controls on the Trajectory of Dune Toe Retreat. *Geomorphology* **2023**, *438*, 108826. [[CrossRef](#)]
55. Saye, S.E.; Van Der Wal, D.; Pye, K.; Blott, S.J. Beach–Dune Morphological Relationships and Erosion/Accretion: An Investigation at Five Sites in England and Wales Using LIDAR Data. *Geomorphology* **2005**, *72*, 128–155. [[CrossRef](#)]
56. Moore, L.J.; Vincent, O.D.; Ruggiero, P. Vegetation Control Allows Autocyclic Formation of Multiple Dunes on Prograding Coasts. *Geology* **2016**, *44*, 559–562. [[CrossRef](#)]
57. Silva, R.; Martínez, M.L.; Odériz, I.; Mendoza, E.; Feagin, R.A. Response of Vegetated Dune–Beach Systems to Storm Conditions. *Coast. Eng.* **2016**, *109*, 53–62. [[CrossRef](#)]
58. Bauer, B.O.; Hesp, P.A.; Smyth, T.A.G.; Walker, I.J.; Davidson-Arnott, R.G.D.; Pickart, A.; Grilliot, M.; Rader, A. Air Flow and Sediment Transport Dynamics on a Foredune with Contrasting Vegetation Cover. *Earth Surf. Process. Landf.* **2022**, *47*, 2811–2829. [[CrossRef](#)]
59. Keijzers, J.G.S.; De Groot, A.V.; Riksen, M.J.P.M. Vegetation and Sedimentation on Coastal Foredunes. *Geomorphology* **2015**, *228*, 723–734. [[CrossRef](#)]
60. Shumack, S.; Farebrother, W.; Hesse, P. Quantifying Vegetation and Its Effect on Aeolian Sediment Transport: A UAS Investigation on Longitudinal Dunes. *Aeolian Res.* **2022**, *54*, 100768. [[CrossRef](#)]
61. O’Connell, J. Coastal Dune Protection & Restoration: Using ‘Cape’ American Beachgrass & Fencing 2008. Available online: <https://repository.library.noaa.gov/view/noaa/42104> (accessed on 1 May 2022).
62. Passeri, D.L.; Dalyander, P.S.; Long, J.W.; Mickey, R.C.; Jenkins, R.L.; Thompson, D.M.; Plant, N.G.; Godsey, E.S.; Gonzalez, V.M. The Roles of Storminess and Sea Level Rise in Decadal Barrier Island Evolution. *Geophys. Res. Lett.* **2020**, *47*, e2020GL089370. [[CrossRef](#)]
63. van Wiechen, P.P.J.; de Vries, S.; Reniers, A.J.H.M.; Aarninkhof, S.G.J. Dune Erosion during Storm Surges: A Review of the Observations, Physics and Modelling of the Collision Regime. *Coast. Eng.* **2023**, *186*, 104383. [[CrossRef](#)]
64. Suanez, S.; Cancouët, R.; Floc’h, F.; Blaise, E.; Ardhuin, F.; Filipot, J.-F.; Cariolet, J.-M.; Delacourt, C. Observations and Predictions of Wave Runup, Extreme Water Levels, and Medium-Term Dune Erosion during Storm Conditions. *JMSE* **2015**, *3*, 674–698. [[CrossRef](#)]
65. Smart, L.S.; Vukomanovic, J.; Sills, E.O.; Sanchez, G. Cultural Ecosystem Services Caught in a ‘Coastal Squeeze’ between Sea Level Rise and Urban Expansion. *Glob. Environ. Chang.* **2021**, *66*, 102209. [[CrossRef](#)]
66. Ranasinghe, R.; Callaghan, D.P.; Li, F.; Wainwright, D.J.; Duong, T.M. Assessing Coastline Recession for Adaptation Planning: Sea Level Rise versus Storm Erosion. *Sci. Rep.* **2023**, *13*, 8286. [[CrossRef](#)] [[PubMed](#)]
67. Moulton, M.A.B.; Hesp, P.A.; Miot Da Silva, G.; Keane, R.; Fernandez, G.B. Surfzone-Beach-Dune Interactions along a Variable Low Wave Energy Dissipative Beach. *Mar. Geol.* **2021**, *435*, 106438. [[CrossRef](#)]
68. Ajedegba, J.O.; Choi, J.-W.; Jones, K.D. Analytical Modeling of Coastal Dune Erosion at South Padre Island: A Consideration of the Effects of Vegetation Roots and Shear Strength. *Ecol. Eng.* **2019**, *127*, 187–194. [[CrossRef](#)]
69. Charbonneau, B.R.; Duarte, A.; Swannack, T.M.; Johnson, B.D.; Piercy, C.D. DOONIES: A Process-Based Ecogeomorphological Functional Community Model for Coastal Dune Vegetation and Landscape Dynamics. *Geomorphology* **2022**, *398*, 108037. [[CrossRef](#)]
70. Nadal-Caraballo, N.C.; Melby, J.A.; Gonzalez, V.M.; Cox, A.T. *Coastal Storm Hazards from Virginia to Maine*; Project 401426, North Atlantic Coast Comprehensive Study; U.S. Army Engineer Research and Development Center; Coastal and Hydraulics Laboratory: Vicksburg, MS, USA, 2015.

Disclaimer/Publisher’s Note: The statements, opinions and data contained in all publications are solely those of the individual author(s) and contributor(s) and not of MDPI and/or the editor(s). MDPI and/or the editor(s) disclaim responsibility for any injury to people or property resulting from any ideas, methods, instructions or products referred to in the content.